Atomistic computer simulations of yttrium iron garnet (YIG) as an approach to materials defect chemistry. I. Intrinsic defects

1993 J. Phys.: Condens. Matter 5 2947

(http://iopscience.iop.org/0953-8984/5/18/017)

J. Phys.: Condens. Matter 5 (1993) 2947–2960. Printed in the UK

Atomistic computer simulations of yttrium iron garnet (YIG) as an approach to materials defect chemistry: I. Intrinsic defects

H Donnerberg† and C R A Catlow‡

† Fachbereich Physik, Universität Osnabrück, PO Box 4469, D-4500 Osnabrück, Germany

‡ Davy Faraday Research Laboratory, Royal Institution, London W1X 4BS, Great Britain

Received 11 January 1993, in final form 15 February 1993

Abstract. In this paper we report results of atomistic simulation studies of the formation of intrinsic defect structures in YIG. Using calculated defect formation energies we obtain energies for defect reactions, from which we determine the most favourable defect processes in yttrium iron garnet. Finally, we comment on some electronic properties of YIG crystals.

1. Introduction

Garnet crystals are well known to play an important role in technological devices. For example, yttrium aluminium garnet (YAG) doped with Nd^{3+} ions is one of the most commonly used laser materials. Other examples are provided by magnetic garnets, of which ferrimagnetic yttrium iron garnet (YIG) represents the most prominent member, with YIG devices used extensively in various microwave applications [1].

Recent developments concern the construction of magneto-optical device components for their use in integrated optics based on thin YIG films deposited on substrate garnet materials [1–3]. As is generally true for crystalline materials, the basic physical crystal properties (e.g. optical absorption, Faraday rotation and photomagnetic effects) of YIG depend to a considerable extent on its defect structure. For example, Fe^{2+} and Fe^{4+} ions as well as Bi^{3+} dopants are well known to modify strongly the above-quoted magneto-optical crystal properties. Similar influences can be ascribed to Pb^{2+} impurities, which are always present in YIG as part of the usual crystal growth techniques [1]. Garnet crystals are well suited to accommodate many different cation types with various valences and with concentrations in the percentage range [1]. The aim is to optimize the technical properties of the material by controlled impurity incorporation—a procedure that may be described as 'molecular engineering'.

In spite of the extensive experimental work in this field, there is still need for a definite and generally accepted defect model, which covers the basic questions of the dominant intrinsic defects as well as to the incorporation sites and modes of charge compensation of impurity ions.

In this paper we present results of atomistic computer simulation studies on energetically favourable intrinsic point defect structures in YIG and related electronic properties. Impurities will be discussed in a subsequent publication. For two decades simulation methods based on effective potentials have proved to be very effective in elucidating defect structures in ionic and semi-ionic materials [4–6]. The success and scope of the field is evident from recent investigations on complex oxide crystals, such as $BaTiO_3$ [7], $LiNbO_3$ [8, 9], La_2CuO_4 [10, 11] and YAG [12]. These and other studies have clearly shown

0953-8984/93/182947+14$07.50

that the techniques have a predictive capacity in determining the type of defect properties investigated in this paper.

2. Computational details

Our calculations are essentially based on an ionic crystal model. Interactions between crystal ions are specified using pair potentials in the central field approximation. In addition to long-range Coulomb potentials we need to consider short-range potentials as a consequence of the Pauli exclusion principle and interionic electron correlation effects. Short-range ion–ion interactions are described using Buckingham potentials:

$$V(r) = A\,e^{-r/\rho} - C/r^6. \tag{2.1}$$

The electronic polarizability of crystal ions is introduced into our model by means of the shell model of Dick and Overhauser [13]. Thus, crystal ions are described as consisting of an ionic core (charge X, mass M) to which the shell of valence electrons (charge Y, mass O) is coupled via an isotropic harmonic restoring force (force constant K). The formal ionic charge is then given by $Q = X + Y$ and the (free) electronic polarizability by

$$\alpha = Y^2/K. \tag{2.2}$$

It is useful to note that all short-range ion–ion potentials are defined as acting between different ion shells. As a consequence the true electronic polarizability of the ions becomes dependent on the crystal environment—an important physical effect (especially for anions) that is simply and economically described by the shell model. The success of any shell model calculation depends on the quality of the potential (A, ρ, C) and shell (Y, K) parameters and hence on the ability to reproduce the perfect crystal structure as well as the dielectric and elastic constants. Therefore, the usual strategy is to obtain the *a priori* unknown potential parameters by an empirical fitting procedure, although extensive and growing use is made of theoretical procedures in developing short-range potential parameters. In the 'empirical' approach, however, properties of the 'shell model crystal' are adjusted to give the appropriate real crystal properties by treating the unknown parameters as variables.

Having developed a suitable parametrization, this is implemented in the defect simulations, the central idea of which is the use of energy minimization with respect to all ionic core and shell positions resulting in stable crystal configurations for both the perfect and the defective lattice and in defect energies which are used to determine enthalpies of defect chemical reactions. Defect energies are calculated using a two-region-strategy. The inner region around the defect containing 100–300 ions is treated atomistically, whereas polarization effects in the outer region are described by means of the continuum theoretical Mott–Littleton approximation [14]. We emphasize that defect-induced lattice relaxation effects are modelled this way. The features described above are coded in the CASCADE program [15], and further details of computer simulations of solids can be obtained from [4].

In our simulation study on YIG we considered two sets of parameters (table 1). The first (I) has been obtained by transferring empirical shell model parameters from Y_2O_3 and α-Fe_2O_3 [7] to YIG, while the second (II) was derived by empirical fitting to the properties of YIG. In order to keep the number of degrees of freedom per unit cell manageable, the yttrium ions have been defined to be unpolarizable in both parameter sets, both of which

reproduce the observed crystal structure to sufficient accuracy (neglecting slight distortions arising from the ferrimagnetic order in YIG) [1]. Deviations with respect to ion positions are less than 0.05 Å. We note that magnetic interactions mediated by superexchange cannot be accounted for within classical shell model simulations.

Table 1. Shell model parameters according to parameter sets I and II.

Interaction		A (eV)	ρ (Å)	C (eV Å^6)	Ion		Y ($\|e\|$)	k (eVÅ^{-2})
O^{2-}–O^{2-}	I	22764.0	0.149	27.8	O^{2-}	I	−2.811	103.07
	II	22764.0	0.149	87.5		II	−3.148	43.31
Y^{3+}–O^{2-}	I	1345.1	0.3491	0.0	Y^{3+}	I	—	—
	II	1388.0	0.3561	0.0		II	—	—
$Fe^{3+}_{(a)}$–O^{2-}	I	1102.4	0.3299	0.0	$Fe^{3+}_{(a)}$	I	4.97	304.7
	II	993.9	0.3400	0.0		II	5.30	408.0
$Fe^{3+}_{(d)}$–O^{2-}	I	1102.4	0.3299	0.0	$Fe^{3+}_{(d)}$	I	4.97	304.8
	II	852.3	0.3490	0.0		II	4.65	205.0

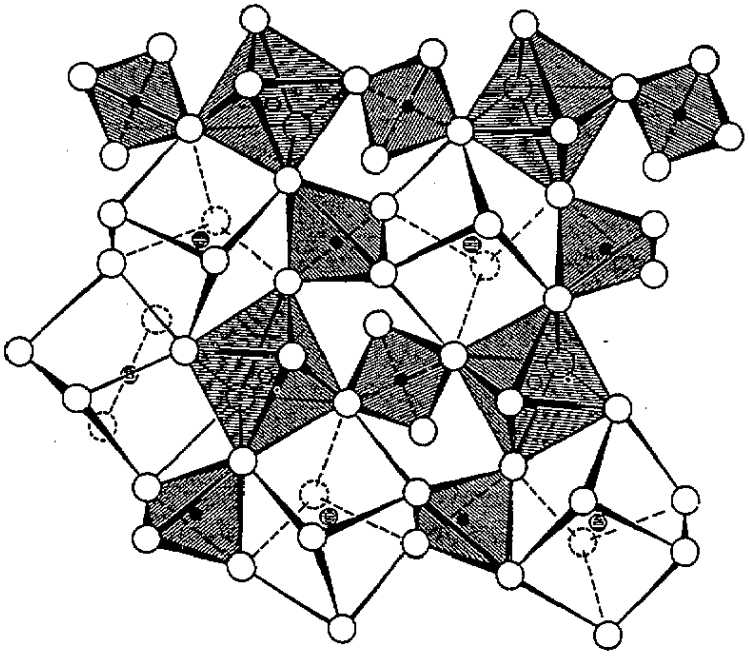

Figure 1. Spatial connection of oxygen polyhedra in garnets. The framework of alternating tetrahedra and octahedra (shaded) and of eightfold dodecahedra is shown. Large open circles represent oxygen ions, small circles cations [1].

Garnet crystals possess a cubic body-centred Bravais lattice belonging to the space group Ia 3d (O_h^{10}). The basis of the lattice consists of four formula units of YIG ($\hat{=}$ $Y_3Fe_5O_{12}$),

where the Y^{3+} ions occupy the 24c dodecahedrally coordinated sites and Fe^{3+} ions both the octahedral 16a sites and the tetrahedral 24d sites. More accurately one should write $(Y_3)_{24c}$ $(Fe_2)_{16a}$ $(Fe_3)_{24d}$ O_{12}. Figure 1 shows the spatial connection of the various oxygen polyhedra in YIG.

By inspection of table 1 we observe that in set II tetrahedrally and octahedrally coordinated Fe^{3+} ions have been assigned different interatomic potential parameters, which appears to be reasonable because of possible changes of cation properties (e.g. ion size) as a function of coordination number. In table 2 we have summarized calculated as well as experimentally determined macroscopic constants. We see that only set II can accurately reproduce the dielectric behavior of YIG, which is of considerable importance in predicting reliable defect energies. All defect energies reported below refer to the parameter set II, except when indicated to the contrary.

Table 2. Comparison of calculated and measured macroscopic constants.

Macroscopic constant	Calculated		Experiment [1, 16]
	I	II	
C_{11}(GPa)	326.0	273.4	268–270.1
C_{12}(GPa)	111.5	129.8	110.6–110.9
C_{44}(GPa)	101.2	68.7	76.6–77.5
ϵ_0	10.3	17.5	$\simeq 17$
ϵ_∞	2.11	5.3	$\simeq 5$

3. Results and discussion

3.1. Some remarks on the chemical stability of YIG

Having demonstrated the success of our potential models in describing structural properties of garnet we continue with a consideration of the extent to which they are compatible with the observed stoichiometry variations and phase relations of the material.

Under most practical conditions the phase diagram appropriate to YIG can be described by the binary Y_2O_3–Fe_2O_3 system. Deviations from this description will only occur if the system is exposed to reducing or oxidizing atmospheres [1, 17]. In this latter case our analysis must include the relevant defect redox reactions.

At the present stage it is sufficient to take advantage of the 'pseudobinary' system, thus to consider reactions of the following type:

$$2Y_3Fe_5O_{12} \longrightarrow 3Y_2O_3 + 5Fe_2O_3 \tag{3.1}$$

or alternatively

$$Y_3Fe_5O_{12} \longrightarrow Fe_2O_3 + 3YFeO_3. \tag{3.2}$$

The energies of reaction can be estimated by combining calculated lattice energies (per formula unit) using the YIG potential parameters (table 1). In (3.2) we have included the perovskite structured yttrium orthoferrite $YFeO_3$, which is readily formed on the yttrium-rich side of the phase diagram. We note also that Y_2O_3, Fe_2O_3 and $YFeO_3$ are fairly well

modelled using the YIG parameters. For example, the calculated lattice constant of $YFeO_3$, $a = 3.863$ Å, is only 0.016 Å larger than the experimental value.

As a result we obtain (per formula unit YIG) +1.56 eV and +2.91 eV for reactions (3.1) and (3.2) respectively. These values show the stoichiometric formation of YIG to be favourable. The same qualitative conclusion is reached if parameter set I is used instead of II.

We conclude this subsection with a few considerations on non-stoichiometry, to which we return later when presenting our defect calculations. We have considered both Y_2O_3 and Fe_2O_3 excess in YIG crystals by modelling $Y_3(Fe_4Y)O_{12}$ and $(Y_2Fe)Fe_5O_{12}$ respectively. Thus, in the first case 1/5 of the Fe in the garnet is replaced by Y, and in the second case 1/3 of the Y is replaced by Fe. This procedure, despite the fact that the compositions show greater Y and Fe excess than observed experimentally, nevertheless allow us to probe the energetics associated with non-stoichiometry. Thus calculations were performed using the parameter sets in table 1 for the following reactions:

$$Y_2O_3 + 3Fe_2O_3 \longrightarrow (Y_2Fe)Fe_5O_{12} \tag{3.3}$$

for which the calculated energy is 1.33 eV and

$$2Y_2O_3 + 2Fe_2O_3 \longrightarrow Y_3(Fe_4Y)O_{12} \tag{3.4}$$

where we calculate −0.77 eV for the energy of reaction.

Whereas Fe_2O_3 excess turns out to be slightly endothermic, Y_2O_3 excess is seen to be exothermic. At first sight this result seems to contradict the observed phase diagram, from which a small possible Fe_2O_3 excess can be inferred but no Y_2O_3 excess. In order to resolve this contradiction we suggest the formation of $YFeO_3$ might be preferred over Y_2O_3-rich YIG. Indeed, by calculation of appropriate lattice energies, and taking into account that one unit of $Y_3(Fe_4Y)O_{12}$ corresponds to four units of $YFeO_3$, we find this interpretation to be reasonable, by reference to the following lattice energies:

$$E_{\mathrm{Latt}}(YFeO_3) = -141.1\,\mathrm{eV}\ (-142.5\,\mathrm{eV})$$
$$\tfrac{1}{4}\,E_{\mathrm{Latt}}\big(Y_3(Fe_4Y)O_{12}\big) = -141.7\,\mathrm{eV}\ (-141.9\,\mathrm{eV})$$

(where energies in brackets refer to parameter set I). We should approach these results with some caution, owing the uncertainties introduced by transferring YIG parameters to different materials as well as by neglecting thermal effects. Nevertheless, the qualitative conclusions are reasonably clear: yttrium excess may be accommodated by formation of the perovskite $YFeO_3$ rather than non-stoichiometric phases, as there is very little difference in the lattice energies of the two phases.

3.2. Intrinsic defect structures

We now discuss point defect formation mechanisms involving yttrium, iron or oxygen ion species only. Impurity point defects will be considered in a later publication.

Table 3 lists the basic defect energies, from which it is straightforward to consider the energetics of Schottky- and Frenkel-type defect formation. In all subsequent reactions we use the defect notation of Kröger and Vink [18]; the symbol 'YIG' denotes the bulk crystal.

Table 3. Basic defect energies using parameter set II.

Defect	Basic defect formation energy (eV)
$V^{3'}_{Fe(a)}$	51.49
$V^{3'}_{Fe(d)}$	50.88
$V^{\cdot\cdot}_{O}$	21.43
$V^{3'}_{Y}$	42.96
Fe^{x}_{Y}	−8.03
$Y^{x}_{Fe(a)}$	9.63
$Y^{x}_{Fe(d)}$	10.57
O''_{I}	−14.32
$Fe^{3\cdot}_{I}$	−39.02
$Y^{3\cdot}_{I}$	−26.05

Table 4. Reaction energies (per defect) for Schottky-like and Frenkel disorder reactions

Disorder reaction	Reaction energy per defect (eV)
Schottky-like	
(3.5)	3.11
(3.6)	3.54
(3.7)	3.19
(3.8)	3.41
Frenkel-like	
(3.9)	5.93
(3.10)	8.45
(3.11)	3.55

Schottky disorder

$$\text{'YIG'} \rightarrow Fe_2O_3 + 2V^{3'}_{Fe} + 3V^{\cdot\cdot}_{O} \tag{3.5}$$

$$\text{'YIG'} \rightarrow Y_2O_3 + 2V^{3'}_{Y} + 3V^{\cdot\cdot}_{O} \tag{3.6}$$

$$\text{'YIG'} \rightarrow Y_3Fe_5O_{12} + 3V^{3'}_{Y} + 5V^{3'}_{Fe} + 12V^{\cdot\cdot}_{O} \tag{3.7}$$

$$\text{'YIG'} \rightarrow YFeO_3 + V^{3'}_{Y} + V^{3'}_{Fe} + 3V^{\cdot\cdot}_{O} \tag{3.8}$$

(where only reaction (3.7) represents true Schottky disorder, as the others result in a change in the chemical composition of the material)

Frenkel disorder

$$\text{'YIG'} \rightarrow V^{3'}_{Fe} + Fe^{3\cdot}_{I} \tag{3.9}$$

$$\text{'YIG'} \rightarrow V^{3'}_{Y} + Y^{3\cdot}_{I} \tag{3.10}$$

$$\text{'YIG'} \rightarrow V^{\cdot\cdot}_{O} + O''_{I}. \tag{3.11}$$

The respective energies are summarized in table 4. We assume the creation of iron vacancies to involve tetrahedral iron sites only, because of the lower defect energies as compared to octahedral sites (see table 3). Even the most favourable defect reactions in table 4 need for their creation the rather large formation energies per defect of about 3.1–3.5 eV respectively. In accordance with previous investigations [7, 8] we thus conclude both Schottky and Frenkel disorder to be insignificant.

Another type of intrinsic disorder may be introduced by interchanging Y^{3+} and Fe^{3+} cations according to

$$Y_Y^x + Fe_{(a)}^x \rightarrow Y_{(a)}^x + Fe_Y^x \tag{3.12}$$

for which we calculate a reaction energy of 0.8 eV per defect. The shortened subscript (a) denotes the octahedral iron site. The comparatively low reaction energy suggests that this type of disorder exists in YIG crystals. We note that the cation interchange specified above does not alter the magnetic moment per formula unit, because the 24c and the 16a sublattices are known to have a parallel spin coupling [1]. We emphasize that the above results refer to otherwise perfectly grown YIG crystals, but as most YIG crystals are known to have considerable impurity concentrations (e.g. Bi^{3+} ions) we should note that the cation interchange energy is further reduced in those crystals where large cations are incorporated. This has been shown, for instance, by simulating the cation interchange in $Y_3(Fe_4Y)O_{12}$ (0.54 eV per defect) and in $(Y_{\frac{2}{4}}Bi_{\frac{3}{4}})Fe_5O_{12}$ (0.70 eV per defect). For modelling of the latter compound a Bi–O short-range interaction potential has been taken over from simulation studies on $BaBiO_3$ [19].

Since antisite defect formation is the lowest energy mode of disorder in these crystals, non-stoichiometry, i. e. Fe_2O_3 or Y_2O_3 excess, would be expected to be mainly accommodated by means of 'antisite' defects, interstitial ions or vacancies:

$$\tfrac{1}{2}Y_2O_3 + \text{'YIG'} \rightarrow Y_{(a)}^x + \tfrac{1}{2}Fe_2O_3 \tag{3.13}$$

$$Y_2O_3 + \text{'YIG'} \rightarrow 2Y_i^{3\cdot} + 3O_i'' \tag{3.14}$$

$$Y_2O_3 + \text{'YIG'} \rightarrow 2YFeO_3 + 2V_{Fe}^{3'} + 3V_O^{\cdot\cdot} \tag{3.15}$$

$$\tfrac{1}{2}Fe_2O_3 + \text{'YIG'} \rightarrow Fe_Y^x + \tfrac{1}{2}Y_2O_3 \tag{3.16}$$

$$Fe_2O_3 + \text{'YIG'} \rightarrow 2Fe_i^{3\cdot} + 3O_i'' \tag{3.17}$$

$$Fe_2O_3 + \text{'YIG'} \rightarrow 2YFeO_3 + 2V_Y^{3'} + 3V_O^{\cdot\cdot}. \tag{3.18}$$

By inspection of table 5 we first infer that formation of interstitial ions and vacancies is energetically unfavourable. Second, it should be noted that in agreement with our previous calculations of chemical stability (section 3.1) an excess of Y_2O_3 is preferred against a surplus Fe_2O_3. However, as we have already discussed in section 3.2, the formation (or phase separation) of yttrium orthoferrite is likely to reduce the occurrence of excess Y_2O_3 in YIG crystals. Experimental evidence for excess Y_2O_3 has only been found in YIG substituted with one aluminium ion per formula unit [20]. Finally, we note that the formation of Fe_Y^x antisites as a result of surplus Fe_2O_3 leads in agreement with experimental data [21] to a decrease of the lattice constant. This might have been expected on the basis of ion size arguments.

In conclusion, we predict Fe_Y^x antisite defects to exist to some extent in each YIG crystal as a result of either cation interchange (reaction (3.12)) or slight Fe_2O_3 non-stoichiometry. Defects of this type are expected to facilitate the reduction of YIG as well as the incorporation of tetravalent impurities. In contrast to the case for Y_2O_3, excess Fe_2O_3 is well known to occur in otherwise pure YIG [21, 22].

Table 5. Energetics of Y_2O_3 and Fe_2O_3 excess in YIG.

Reaction	Reaction energy (eV) per molecule A_2O_3
(3.13)	1.24
(3.14)	37.44
(3.15)	16.43
(3.16)	1.96
(3.17)	29.52
(3.18)	18.61

3.3. Intrinsic electronic properties

We now remark on reduction and oxidation treatments, electrical conductivity and on optical absorption in YIG crystals, within the obvious limitations imposed by treatment based on effective potentials. In our simulation study additional $Fe^{2+/4+}$ ion species have been modelled by appropriately changing the ionic charge state with regard to the intrinsic 3+ state. As the modification of short-range potential parameters, at the same time, is expected to be small, these parameters have been taken to be unaltered.

YIG crystals annealed in atmospheres with low oxygen partial pressure contain additional electrons, which lead to the formation of ferrous ions Fe^{2+}. Even under growth conditions Fe^{2+} ions have been observed in YIG [23]. It has been suggested that these extra charges may be compensated either by oxygen vacancies or by interstitial ions [21]. Our shell model calculations show that oxygen vacancies are more likely to occur:

$$\text{'YIG'} \rightarrow \tfrac{3}{2}O_2(g) + 3V_O^{\cdot\cdot} + 6Fe' \tag{3.19}$$

$$\text{'YIG'} \rightarrow \tfrac{15}{4}O_2(g) + 5Fe_I^{3\cdot} + 15Fe' - Y_3Fe_5O_{12} + \tfrac{3}{2}Y_2O_3 \tag{3.20}$$

where (3.20) represents the most favourable reduction mechanism involving interstitial ions. It should be noted that the interstitial-type reaction needs to resolve one formula unit of YIG from the surface into the bulk lattice. As we have calculated this is energetically rather costly: (3.19) is more favourable by about 6 eV per O_2 molecule than (3.20).

The absolute reduction energies depend on the exact formation energy of Fe^{2+} ions. These may be estimated by combining shell model defect energies with the appropriate ionization energies [24]. If we consider, for example, otherwise perfectly grown YIG we find octahedrally coordinated Fe^{2+} ions by 0.6 eV more favourable than tetrahedrally coordinated Fe^{2+} ions. However, if Fe_Y^x antisite defects are present (e.g. as resulting from non-stoichiometry or from cation interchange discussed above) we find that these defects become the favoured 'traps' for additional electrons. This lowers the reduction energy by a further 4.6 eV per O_2 to give the reaction energy for (3.19) of 11.9 eV per O_2, which is lower by about 25 eV per O_2 than the reduction energy calculated for YAG [12], which is in qualitative agreement with the observation that YIG may to some extent be reduced, but not YAG [12]. In table 6 we summarize binding energies between oxygen vacancies and trapped electrons. In principle the inclusion of such energies can lead to even smaller reduction energies. The last defect complex in table 6 is, however, assumed to be defect chemically insignificant because of the comparatively low concentrations of the constituent defect species. Finally, we note that all reduction mechanisms discussed so far can be used to describe the observed thermal decomposition of YIG that takes place under strong

reducing conditions [25]. For instance, (3.19) can be reformulated as follows:

$$\begin{aligned} 6Y_3Fe_5O_{12} &\rightarrow O_2 + 2V_O^{\cdot\cdot} + 4Fe' + 26Fe_{Fe}^{x} + 18Y_Y^{x} + 70O_O^{x} \\ &\rightarrow O_2 + 18YFeO_3 + 4(Fe' + 2Fe_{Fe}^{x} + 4O_O^{x}) \\ &\rightarrow O_2 + 18YFeO_3 + 4Fe_3O_4. \end{aligned} \tag{3.21}$$

We now turn to oxidation of YIG in oxygen-rich atmospheres; again we first consider perfectly grown YIG crystals, for which we can write the following reaction:

$$O_2(g) + \text{'YIG'} \rightarrow 2O_I'' + 4Fe_{(d)}^{\cdot} \tag{3.22}$$

for which we calculate an energy of 17.6 eV per O_2 molecule which is prohibitively high. However, in most YIG crystals oxygen vacancies will be present, either as frozen in from high-temperature reducing growth conditions, or as charge compensators for divalent impurities. Later oxidation treatments may then be viewed as simply filling oxygen vacancies:

$$4Fe_{(d)}^{x} + O_2(g) + 2V_O^{\cdot\cdot} \rightarrow 2O_O^{x} + 4Fe_{(d)}^{\cdot}. \tag{3.23}$$

The oxidation energy in this latter case is calculated to be 3.3 eV per O_2. We conclude therefore that the oxidation of YIG will have a reasonably low reaction energy only when there is an extrinsic oxygen vacancy population. To complete these results we note that holes at tetrahedral iron sites are more favourable than those at octahedral iron sites (by 4.2 eV) as well as at oxygen sites (by 1.6 eV).

Table 6. Binding energies (eV) of electrons at oxygen vacancies. The binding energy is defined as the reaction energy corresponding to $Fe' + V_O^{\cdot\cdot} \rightarrow (Fe'\ V_O^{\cdot\cdot})$ (complex).

Defect complex	Binding energy (eV)
$(V_O^{\cdot\cdot}\ Fe'_{(a)})$	−0.38
$(V_O^{\cdot\cdot}\ Fe'_{(d)})$	−0.56
$(V_O^{\cdot\cdot}\ Fe'_Y)$	−0.85

Finally, it should be emphasized that our calculated redox reaction energies are very sensitive to the accuracy with which electronic energy terms can be accounted for in shell model simulations (note the amplifying factor of four occurring in (3.19)–(3.23)). Thus, using free-ion ionization energies, it is likely that our redox energies are overestimated by a few eV. Their qualitative importance, however, in predicting the favourable redox processes is obvious as possible shortcomings regarding the electronic structure have been made consistently throughout our work. Moreover, in order to determine the driving forces of redox reactions, i.e. the Gibbs free energy $\Delta G = \Delta H - T\Delta S$, it is necessary to include essential entropy terms because the formation (reduction) or consumption (oxidation) of oxygen gas is involved (e.g. using standard entropy data for oxygen we find $T\Delta S \simeq 2.2$ eV at $T \simeq 600$°C). Thus, $\Delta G < \Delta H$ is obtained in the case of reduction, but $\Delta G > \Delta H$ for oxidation. The inclusion of entropy terms, however, would not influence our qualitative predictions regarding the most favourable reduction and oxidation mechanisms.

Macroscopic crystal properties, such as electrical conductivity and optical absorption, are significantly influenced by the presence of species like Fe^{2+} and Fe^{4+} ions. We may investigate these species by means of shell model calculations, which have the advantage that lattice relaxation effects are properly taken into account. Quantum mechanical terms, on the other hand, can only be considered in a very approximate way by addition of appropriate free-ion ionization energies and (where necessary) crystal field stabilization energies. A shell model treatment of electron or hole species necessarily implies a small-polaron model. The stability condition favouring small polarons is given by

$$|E_B| > \tfrac{1}{2}\Delta \tag{3.24}$$

where E_B means the small-polaron binding energy and Δ the appropriate band-width. The right-hand side of (3.24) represents the gain in delocalization energy in a band model, which may be considered to be competitive with small-polaron formation. In the case of electrons the bandwidth $\Delta = 0.6\,\text{eV}$ is derived from the octahedral t_{2g} (Fe^{2+}) states [26]. For the small-polaron binding energy, which is determined from the lattice relaxation around an octahedrally coordinated Fe^{2+}, we calculate $|E_B| = 1.3\,\text{eV}$; this value is the difference between the energy calculated with full lattice relaxation and that obtained when only shells are allowed to relax and the cores (representing the nuclei) are frozen. If we further include the crystal field splitting energy and its dependence upon nearest-neighbour distances ($10DQ \propto (r_{ML})^{-5}$)$|E_B|$ is finally reduced to about 1.18 eV assuming $10DQ \simeq 1\,\text{eV}$ for the optical (unrelaxed) case and taking into account the calculated outward displacement of the oxygen ligands ($\simeq 0.15$ Å) in the fully relaxed (thermal) case. Thus, on the basis of (3.24) we conclude the small electron polaron to be stable in pure YIG. We should emphasize that the reliability of the calculated binding energy E_B depends to a large extent on the ability of our shell model parameter set (II) to model the dielectric properties of YIG with sufficient accuracy.

Consequently, we expect polaron hopping to represent the dominant electronic conductivity mechanism in YIG. However, it seems difficult to prove this conjecture experimentally as well as theoretically. First, there is a considerable scatter in measured conductivity data resulting from differing experimental conditions regarding the precise chemical composition and type of the YIG samples, the growth conditions and the experimental techniques employed, etc. The conductivity activation energy is found to vary between $\simeq 0.3\,\text{eV}$ to $\simeq 1.8\,\text{eV}$ [1]. Very careful conductivity measurements have been done in case of Si-doped YIG single crystals [26]. The authors interpreted the conductivity activation energy (0.3 eV) as the binding energy of electrons at Si^{4+} dopant ions with no appreciable contributions from mobility activation ($< 0.1\,\text{eV}$) which led to the assumption of band-like electrons. Next, we should recall that small-polaron theories provide different regimes of possible polaron hopping depending on temperature, phonon energies, adiabaticity and on jump correlations [27–29]. As a result, in some cases drift and Hall mobilities need not manifest a clear thermally activated behavior. Thus, the experimentally determined absence of mobility activation, as was claimed in Si-doped YIG, cannot definitely prove the non-existence of small polarons.

Anticipating the validity of the non-adiabatic hopping regime in the high-temperature limit [27] we are able to calculate an upper bound for the polaron hopping activation energy in (pure) YIG. We find $E_H = 0.6\,\text{eV}$ following the approach of Norgett and Stoneham [30], in which the saddle-point energy is obtained by first distributing the electron charge equally over the two neighbouring cation sites and allowing the lattice to relax to equilibrium. This configuration is then frozen and the energy recalculated with the electron localized on one

of the sites. This value is in good agreement with the prediction $E_H = \frac{1}{2}|E_B|$ from the Holstein 'molecular crystal model' [31]. It is, however, too large compared with the results for Si-doped YIG [26] indicating the non-adiabatic high-temperature regime is probably not applicable in this case.

Beyond the 'mobility problem' we have, as in the case of band-like electrons, to consider possible electron traps leading to an additional contribution to the activation energy related to the charge carrier concentration. Intrinsic trapping centres are provided by oxygen vacancies $V_O^{\cdot\cdot}$ (mainly resulting from prior reduction treatments or possibly from charge compensation of divalent impurities) and by Fe_Y^x antisite defects. Thus, the reactions

$$(V_O^{\cdot\cdot}Fe'_{(a)}) \rightarrow V_O^{\cdot\cdot} + Fe'_{(a)} \tag{3.25a}$$

$$Fe^x_{(a)} + Fe'_Y \rightarrow Fe'_{(a)} + Fe^x_Y \tag{3.25b}$$

define corresponding electronic charge-carrier activation modes. The reaction energies are calculated to be 0.38 eV for (3.25*a*) (see table 6) and 1.16 eV for (3.25*b*). The actual charge-carrier activation energies depends not only on these reaction energies but also on the ratio of the numbers of charge carriers and intrinsic defects. We further note that the reaction energy for (3.25*b*) has been calculated neglecting corrections due to crystal field splittings and other electronic energy contributions, which are not accounted for within the shell model. If, for example, the crystal field splitting of Fe_Y antisites is to some extent smaller than the corresponding term of $Fe_{(a)}$ ions, the reaction energy for (3.25*b*) may be substantially lower than our calculated value. As discussed above we predict, in particular, the Fe_Y antisite defects to exist in most YIG crystals with significant contributions.

Extrinsic trapping centres are given by higher-valent impurity ions as Si^{4+}. The conductivity activation energy of 0.3 eV for Si-YIG [26] has been interpreted as the binding energy of $(Si^{\cdot}_{(d)}\ Fe'_{(a)})$ defect complexes. Our calculated binding energy of 0.28 eV provides some support for this interpretation. Again we emphasize that this interpretation may be consistent with both the band electron and the small-polaron model. Further investigations are necessary in order to clarify this point.

In the case of holes as the dominating charge carriers we are uncertain concerning the existence of small-hole polarons, because the appropriate valence bandwidth is not known exactly. It has been estimated as $\simeq 4$ eV [35]. However, the bandwidth should be greater than 6 eV if band-like holes are to be predicted. Our calculated small-hole polaron binding energy is $|E_B| \simeq 3$ eV. We note that correspondingly large valence bandwidths are characteristic of several oxides [36], e.g. MgO (6.5 eV), TiO_2 (5.5 eV), VO_2 (5.6 eV) and Sr TiO_3 (6.5 eV).

In order to complete our investigations on basic electronic properties in YIG we present results concerning optical absorption related to electron/hole transfer between different ions. Once more we use shell model defect energies appropriately corrected by ionization and crystal field energies. We emphasize that all absorption energies subsequently reported mainly yield qualitative guidance for interpretations and should not be taken quantitatively. This, of course, would demand us to include explicitly the electronic structure by means of exact quantum mechanical procedures. As far as local defect electronic properties are concerned, improvements could be achieved by performing embedded-cluster calculations, where one combines an MO description for the inner defective region with a shell model simulation of the outer crystal area [37]. We defer such investigations to the future. Similar comments also apply to some extent to our investigations related to conductivity, as discussed above. However, in that case, in contrast to the present optical calculations, lattice relaxation effects are *fully* taken into account and these dominant terms may outweigh the

uncertainties due to the inaccuracy in treating the electronic structure. Thus thermal energies are expected to be quantitatively more reliable than optical energies.

Table 7. Optical absorption processes. Appropriate shell model energies have been combined with crystal field corrections [30].

Absorption process	Absorption energies (eV) based on the shell model
Electron transfer between iron pairs	
$Fe^{x}_{(a)} + Fe^{x}_{(d)} \rightarrow Fe'_{(d)} + Fe^{\cdot}_{(a)}$	11.12
$Fe^{x}_{(d)} + Fe^{x}_{(a)} \rightarrow Fe^{\cdot}_{(d)} + Fe'_{(a)}$	7.02
$2Fe^{x}_{(a)} \rightarrow Fe^{\cdot}_{(a)} + Fe'_{(a)}$	11.02
$2Fe^{x}_{(d)} \rightarrow Fe^{\cdot}_{(d)} + Fe'_{(d)}$	9.65
Charge transfer, $O^{2-} \rightarrow Fe^{3+}$	
$Fe^{x}_{(a)} + O^{x}_{O} \rightarrow Fe'_{(a)} + O^{\cdot}_{O}$	9.09
$Fe^{x}_{(d)} + O^{x}_{O} \rightarrow Fe'_{(d)} + O^{\cdot}_{O}$	9.83
$Fe^{x}_{Y} + O^{x}_{O} \rightarrow Fe'_{Y} + O^{\cdot}_{O}$	7.24
Absorption related to surplus electrons and holes	
$Fe'_{(a)} + Fe^{x}_{(a)} \rightarrow Fe^{x}_{(a)} + Fe'_{(a)}$	2.67
$Fe'_{(a)} + Fe^{x}_{(d)} \rightarrow Fe^{x}_{(a)} + Fe'_{(d)}$	3.06
$Fe'_{Y} + Fe^{x}_{(d)} \rightarrow Fe^{x}_{Y} + Fe'_{(d)}$	4.10
$Fe'_{Y} + Fe^{x}_{(a)} \rightarrow Fe^{x}_{Y} + Fe'_{(a)}$	3.60
$Fe^{\cdot}_{(d)} + Fe^{x}_{(d)} \rightarrow Fe^{x}_{(d)} + Fe^{\cdot}_{(d)}$	5.78
$Fe^{\cdot}_{(d)} + Fe^{x}_{(a)} \rightarrow Fe^{x}_{(d)} + Fe^{\cdot}_{(a)}$	8.32

In table 7 we summarize various optical absorption energies as calculated on the basis of the shell model. All lattice positions of the ion cores have been held fixed during the absorption processes denoted in table 7. We note that all lattice configurations correspond exactly to the initial states. Thus, in all cases initially involving defects, the appropriate lattice geometry is that of the relaxed initial defect configuration. Only ion shells (representing valence electrons) are allowed to move during absorption processes.

The qualitative features we wish to emphasize here concern the following.

First, the charge transfer processes between oxygen and iron ions show similar absorption energies as those between pairs of iron ions.

Second, the energy gap is determined by the iron pair process:

$$Fe^{x}_{(a)} + Fe^{x}_{(d)} \rightarrow Fe'_{(a)} + Fe^{\cdot}_{(d)}.$$

Third, an absorption band close to the fundamental absorption (gap) is predicted to stem from charge transfer between oxygen and Fe_Y antisite defects.

Fourth, excess electrons and holes essentially lead to optical absorptions within the gap region. Hole transfer needs more energy than electron transfer. The ordering of absorption energies agrees with that corresponding to conductivity activation energies for n- and p-type YIG crystals respectively [1].

Finally, we note that our assignment of the electronic gap is in line with photoconductivity [38] and electrical conductivity [26] measurements.

4. Conclusions

Shell model simulations based on a pair-potential approach are successful in elucidating dominating intrinsic-defect structures in YIG crystals. As a result of deviation from non-stoichiometry and cation interchange reactions we predict that Fe_Y antisite defects play an important role in the materials defect chemistry. Reduction energies, for instance, are significantly lowered by trapping electrons at these antisite defects. In comparison, Schottky and Frenkel disorder are calculated to be only of minor importance.

Investigations on electrical properties provide insight into electrical conductivity mechanisms (small polarons against band electrons) as well as qualitative features of the optical absorption spectra. Thus, we predict the formation of small electron polarons to be favourable in otherwise pure YIG—a result that is reasonable in the light of measured small mobilities and of the small conduction band width. The properties of hole states are more uncertain, but we have shown holes on tetrahedral iron sites to be more favourable than on oxygen sites.

Acknowledgments

We are grateful to the Deutscher Akademischer Austauschdienst, the British Council and to the Deutsche Forschungsgemeinschaft (SFB 225) for financial support of this work. We also thank Professor H Dötsch and Professor O F Schirmer for valuable discussions.

References

[1] Winkler 1981 *Magnetic Garnets (Vieweg Tracts in Pure and Applied Physics)* (Wiesbaden: Vieweg)
[2] Hemme H, Dötsch H and Menzler H P 1987 *Appl. Optics* **26** 3811
[3] Hemme H, Dötsch H and Hertel P 1990 *Appl. Optics* **29** 2741
[4] Catlow C R A and Mackrodt W C (eds) 1982 *Computer Simulation of Solids (Lecture Notes in Physics* **166**) (Berlin: Springer)
[5] Tomlinson S M, Freeman C M, Catlow C R A, Donnerberg H and Leslie M 1989 *J. Chem. Soc. Faraday Trans.* **85** 367
[6] Catlow C R A, Freeman C M, Islam M S, Jackson R A, Leslie M and Tomlinson S M 1988 *Phil. Mag.* A **58** 123
[7] Lewis G V and Catlow C R A 1985 *J. Phys. C: Solid State Phys.* **18** 1149
[8] Donnerberg H, Tomlinson S M, Catlow C R A and Schirmer O F 1989 *Phys. Rev.* B **40** 11909
[9] Donnerberg H, Tomlinson S M, Catlow C R A and Schirmer O F 1991 *Phys. Rev.* B **44** 4877
[10] Allan N L and Mackrodt W C 1988 *Phil. Mag.* A **58** 555
[11] Islam M S, Leslie M, Tomlinson S M and Catlow C R A 1988 *J. Phys. C: Solid State Phys.* **21** L109
[12] Schuh L, Metselaar R and Catlow C R A 1991 *J. Europ. Ceram. Soc.* **7** 67
[13] Dick B G and Overhauser A W 1958 *Phys. Rev.* **112** 90
[14] Mott N F and Littleton M J 1938 *Trans. Faraday Soc.* **34** 485
[15] Leslie M 1983 *Solid State Ionics* **8** 243
[16] Haussühl S, Mateika D Tolksdorf W 1976 *Z. Naturforschg.* **31** 390
[17] Nielsen J W and Dearborn E F 1958 *J. Phys. Chem. Sol.* **5** 202
[18] Kröger F A and Vink H J 1956 *Solid State Physics* **3** ed. F Seitz and D Turnbull (New York: Academic)
[19] Donnerberg H unpublished
[20] MacChesney J B and Potter J F 1965 *J. Amer. Ceram. Soc.* **48**
[21] Metselaar R and Huyberts M A H 1973 *J. Phys. Chem. Sol.* **34** 2257
[22] Paladino A E and Maguire E A 1970 *J. Amer. Ceram. Soc.* **53** 98
[23] Larsen P K and Metselaar R 1975 *J. Solid State Chem.* **12** 253
[24] Weast R C (ed) 1982 *Handbook of Chemistry and Physics* (Boca Raton, FL: CRC Press)
[25] Kimizuka N and Katsura T 1975 *J. Solid State Chem.* **13** 176

[26] Larsen P K and Metselaar R 1976 *Phys. Rev.* B **14** 2520
[27] Böttger H and Bryksin V V 1976 *Phys. Status Solidi* **78** 415
[28] Nagels P 1980 *The Hall Effect and its Applications* ed. C L Chien and C R Westlake (New York: Plenum)
[29] Emin D 1971 *Phys. Rev.* B **3** 1321
[30] Norgett M J and Stoneham A M 1973 *J. Phys. C: Solid State Phys.* **6** 229
[31] Holstein T 1959 *Ann. Phys., NY* **8** 325
[32] Metselaar R and Larsen P K 1974 *Solid State Commun.* **15** 291
[33] Scott G B, Lacklison D E and Page J L 1974 *Phys. Rev.* B **10** 971
[34] Larsen P K and Robertson J M 1974 *J. Appl. Phys.* **45** 2867
[35] Wemple S H, Blank S L, Seman J A and Biolsi W A 1974 *Phys. Rev.* B **9** 2134
[36] Kowalczyk S P, McFeely F R, Ley L, Gritsyna V T and Shirley D A 1977 *Solid State Commun.*
[37] Vail J M 1990 *J. Phys. Chem. Sol.* **51** 589
[38] Grant P M and Ruppel W 1967 *Solid State Commun.* **5** 543